ISBN: 978-3-95450-230-1 ISSN: 2673-5350 doi:10.18429/JACoW-IBIC2021-TUPP10

DEVELOPMENT OF A BEAM HALO MONITOR USING VISIBLE SYNCHROTRON RADIATION AT DIAMOND LIGHT SOURCE

E. Howling*, L. Bobb, Diamond Light Source, Oxford, UK

Abstract

A Beam Halo Monitor (BHM) has been developed at Diamond Light Source (DLS). It is an optical system that uses visible synchrotron radiation (SR) to image the beam halo. In this paper, the design of the monitor is presented, including the introduction of a Lyot stop system to reduce diffraction effects. The BHM was used to take images of a source point of visible SR from a dipole at DLS. These images were analysed to investigate the beam halo and determine the limitations of the monitor. These results will help inform the design of the visible light extraction system and any future BHMs for Diamond-II.

INTRODUCTION

Diamond Light Source (DLS) is a third generation synchrotron light source. In the storage ring, most electrons in the beam reside in the beam core. Due to Touschek and gas scattering some are offset from the core and form a beam halo [1].

Synchrotron radiation from bending magnet sourcepoints at visible and X-ray wavelengths is commonly used for beam diagnostics. X-ray pinhole cameras are used to image the beam core for transverse profile measurements [2]. However, these do not have a great enough dynamic range to image the beam halo, as the halo is approximately 10^{-5} times as bright as the core. Furthermore, the beam core cannot be imaged using visible SR due to the diffraction limit. However, the beam halo is large enough to be imaged with visible SR [3].

A Beam Halo Monitor (BHM) has been developed to better understand the formation and properties of the beam halo. In circular colliders, damping rings and synchrotron light sources, beam halo is one of the critical issues limiting the performance as well as potentially causing component damage and activation [1]. In the case of synchrotron light sources, the beam core determines characteristic parameters such as brightness for beamlines. Therefore a significant beam halo is undesirable. This becomes all the more important upon considering planned synchrotron upgrades, such as Diamond-II [4], where increased brightness for beamline experiments is a key performance indicator.

Given the reduced emittance in Diamond-II, the beam core will be focused to a greater particle density and therefore will exhibit a greater rate of Touschek scattering [5]. These properties of the Diamond-II storage ring mean the beam halo is likely to be more significant than in the current machine. Thus it is beneficial to understand how we expect the beam halo to behave and how it could be observed.

Similar projects have previously been undertaken, including the successful development of a coronagraph BHM at KEK [3]. A similar design was tested at CERN, where it was able to distinguish the halo from the core of a test lamp with a dynamic range of 10^7 [6]. A coronograph BHM was also designed using a micro mirror array to mask the beam core and tested at the University of Maryland Electron Ring [7, 8] and at DLS in collaboration with The Cockcroft Institute.

* Emily.Howling.2017@live.rhul.ac.uk

THE BEAM HALO MONITOR

Stage 1: Design and Installation

A BHM was designed to use visible SR emitted from a dipole magnet to image the beam halo, as shown in Fig. 1. The objective lens is a BORG77EDII apochromat, the characteristics of which are given in Table 1.

Table 1: Characteristics of the BORG77EDII Lens [10]

Parameter	Value
Aperture	77 mm
Focal length	510 mm
F ratio	6.6

Table 2: Properties of the Mako G-319B Camera with a Sony IMX265 Progressive Scan CMOS Sensor [11]

Parameter	Value
Pixels (H × V)	2048 × 1544
Pixel size (H × V)	3.45 × 3.45 µm
Sensing area (H × V)	7.1 × 5.3 mm
Pixel depth	8/12 bit
Shutter type	global
Resolution	3.20 MegaPixels
Max frame rate	37.50 fps

An image of the sourcepoint is formed on a Mako G-319B camera, which uses a Complementary Metal-Oxide-Semiconductor (CMOS) sensor, the properties of which are given in Table 2. Using a CMOS sensor allows the pixels imaging the beam core to saturate without blooming effects ruining the image [9]. The visible SR is a direct representation of the distribution of the electrons at the sourcepoint.

The monitor was built and tested in the lab. A system of mirrors was set up to replicate the 7.37 m optical path from the sourcepoint to the lens, and images taken of a 1951 USAF target were used to characterise the system. Using QuickMTF software [12], the modulation transfer function (MTF) of the system was measured. The properties of the stage 1 beam halo monitor are shown in Table 3.

The monitor was installed in the storage ring, next to the visible light extraction line. Reference images of the

Content from this work may be used under the terms of the CC BY 3.0 licence (© 2021). Any distribution of this work must maintain attribution to the author(s), title of the work, publisher, and DOI

ISBN: 978-3-95450-230-1 ISSN: 2673-5350 doi:10.18429/JACoW-IBIC2021-TUPP10

Content from this work may be used under the terms of the CC BY 3.0 licence (© 2021). Any distribution of this work must maintain attribution to the author(s), title of the work, publisher, and DOI

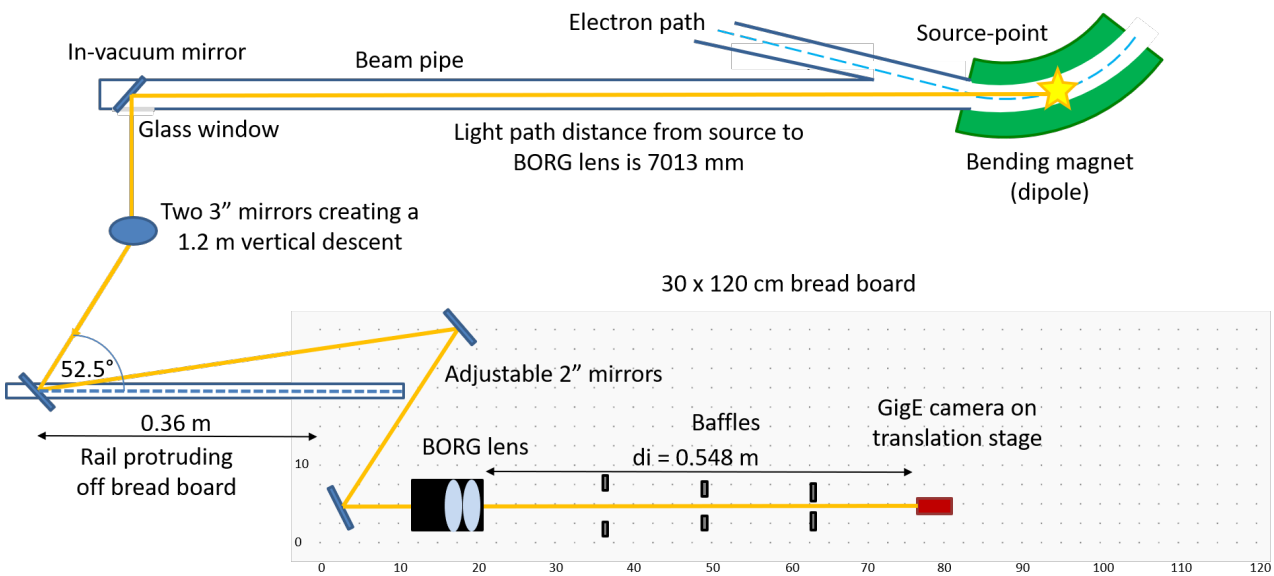

Figure 1: Schematic showing the set up of the stage 1 BHM in the storage ring, not to scale.

Table 3: Table Showing the Properties of the Stage 1 Beam Halo Monitor, as Characterised in the Lab

Parameter	Value
Magnification	−0.0743
Clear aperture	19.8 mm
FOV (H × V)	(56 × 52) ±2 mm
MTF50	0.10587 c/p
MTF10	0.26114 c/p
Depth of focus	0.6864 mm

In-Vacuum Mirror (IVM) were taken using ambient illumination through the viewport. From these images, the orientation of the sourcepoint image relative to the global horizontal and vertical axes of the storage ring could be identified, as shown in Fig. 2.

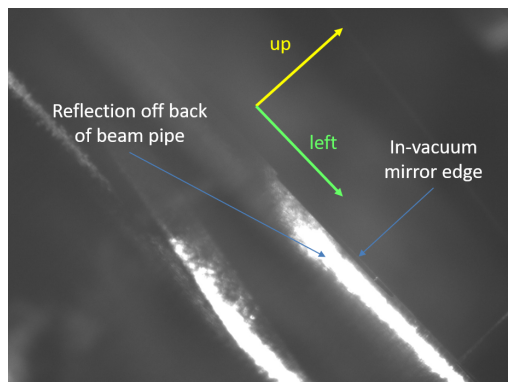

Figure 2: Reference image of the in-vacuum mirror taken using the stage 1 beam halo monitor.

Stage 1: Results

A longitudinal scan of the camera on the 100 mm translation stage was used to determine the optimal position for imaging at constant camera gain and exposure. The optimal position is taken to be that with the maximum intensity.

Images of the sourcepoint were taken at a range of exposures. An example is shown in Fig. 3 where a significant diffraction pattern is observed. The cross shape of the pattern suggests diffraction from a rectangular aperture. Given that the IVM is the only element with a rectangular aperture in the optical path, it was concluded that the diffraction pattern was caused by the this element. Since this mirror cannot be altered, ways to mitigate the diffraction contribution were explored.

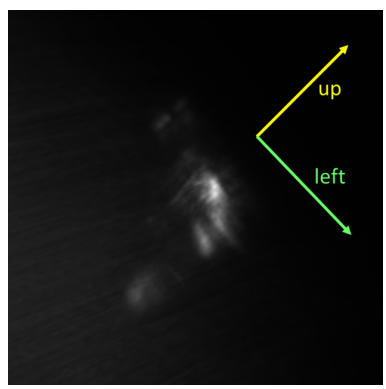

Figure 3: Image of the sourcepoint, region of interest, taken using the stage 1 beam halo monitor with camera gain of 4 dB and a camera exposure time of 893 µs. There is a diffraction pattern below and to the right of the beam core caused by the in-vacuum mirror edges.

Stage 2: Including a Lyot Stop

It is preferable to minimise the diffraction contribution to the acquired image, rather than opting for complex background subtraction via post-processing. To reduce the diffraction contribution using hardware, a Lyot stop system was incorporated into the BHM. A Lyot stop system uses an objective lens to image the source, followed by a field lens to

ISBN: 978-3-95450-230-1 ISSN: 2673-5350 doi:10.18429/JACoW-IBIC2021-TUPP10

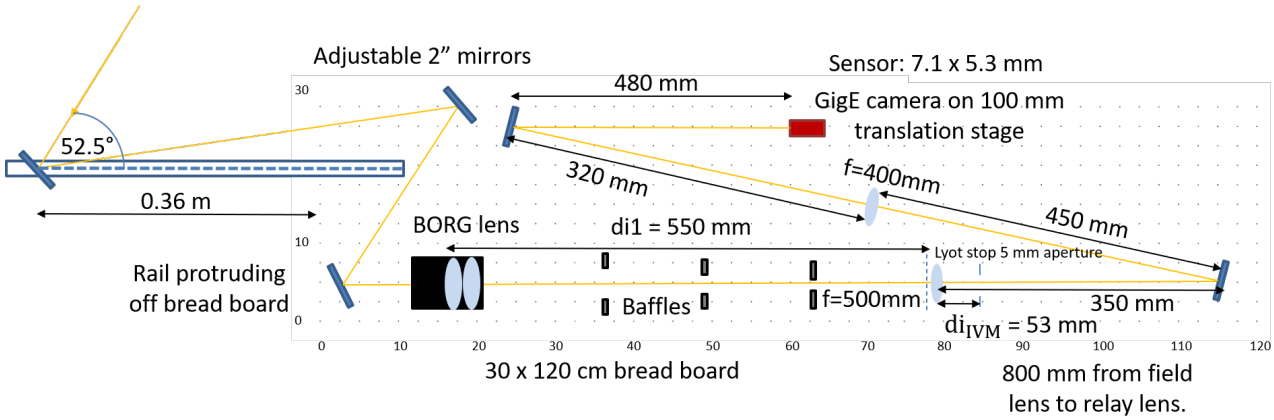

Figure 4: Schematic of the stage 2 beam halo monitor.

image the element causing the diffraction, which is usually the objective lens [3]. This essentially pushes the diffraction pattern to the edge of the image of the diffracting aperture. A Lyot stop is an aperture that then blocks the diffraction pattern. Finally, a relay lens relays the image of the source to the camera. This principle is summarised in the schematic shown in Fig. 5.

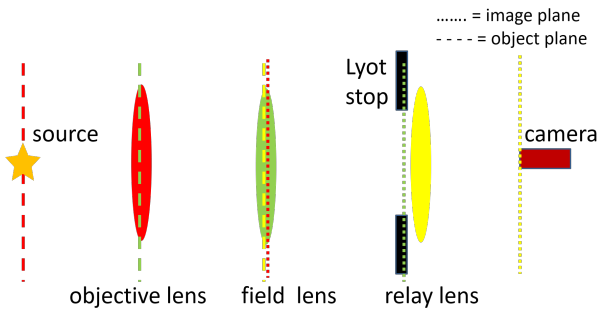

Figure 5: Schematic showing the principle of a Lyot stop system.

At DLS, the diffraction observed in the BHM is not predominately caused by the objective lens, but by the IVM which is 3.13 m upstream of the objective lens. Therefore an adapted Lyot stop was incorporated to suppress the diffraction contribution from the IVM. A schematic of the design for the stage 2 BHM is shown in Fig. 4.

The BHM was upgraded from stage 1 to stage 2 in-situ within the storage ring tunnel. Figure 6 shows an image taken by the stage 2 BHM. Images taken with stage 2 showed a significant suppression of the point spread function from diffraction at the IVM. However, the remaining diffraction pattern is still a major contribution to the background.

ANALYSIS

Images of the sourcepoint were taken at different exposures. The electron beam current was 300±2 mA. The electron beam core had a Gaussian distribution with horizontal and vertical beam sizes of 44.7 µm and 19.5 µm respectively.

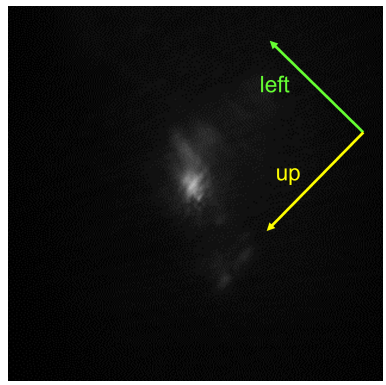

Figure 6: Image of the sourcepoint, region of interest, taken by the stage 2 BHM, with camera gain of 4 dB and a camera exposure time of 893 µs. It shows a signification reduction in the point spread function caused by diffraction from the IVM compared to Fig. 3.

These images were analysed using Matlab [13]. The 'makehdr' function was used to combine the images acquired over a range of camera exposures into High Dynamic Range (HDR) images, allowing both the beam core and the beam halo to be resolved. Cross sections through the centre of the sourcepoint in the HDR images were taken, as shown in Fig. 7. The cross sections were taken in the horizontal and vertical planes, as close as possible to the centre of the beam core, whilst also avoiding the areas of the image most significantly affected by the diffraction pattern caused by the IVM. The cross sections showed a Gaussian beam core and tails either side caused by the beam halo. However the background, predominately caused by the diffraction from the IVM is still too significant to reach meaningful conclusions about the extent of the beam halo.

CONCLUSION

A beam halo monitor has been developed at DLS to investigate whether the beam halo caused by gas and Touschek scattering can be imaged, as a possible diagnostic to investigate these phenomena. This has particular relevance for future lower emittance machines like Diamond-II in which

Content from this work may be used under the terms of the CC BY 3.0 licence (© 2021). Any distribution of this work must maintain attribution to the author(s), title of the work, publisher, and DOI

ISBN: 978-3-95450-230-1 ISSN: 2673-5350 doi:10.18429/JACoW-IBIC2021-TUPP10

Content from this work may be used under the terms of the CC BY 3.0 licence (© 2021). Any distribution of this work must maintain attribution to the author(s), title of the work, publisher, and DOI

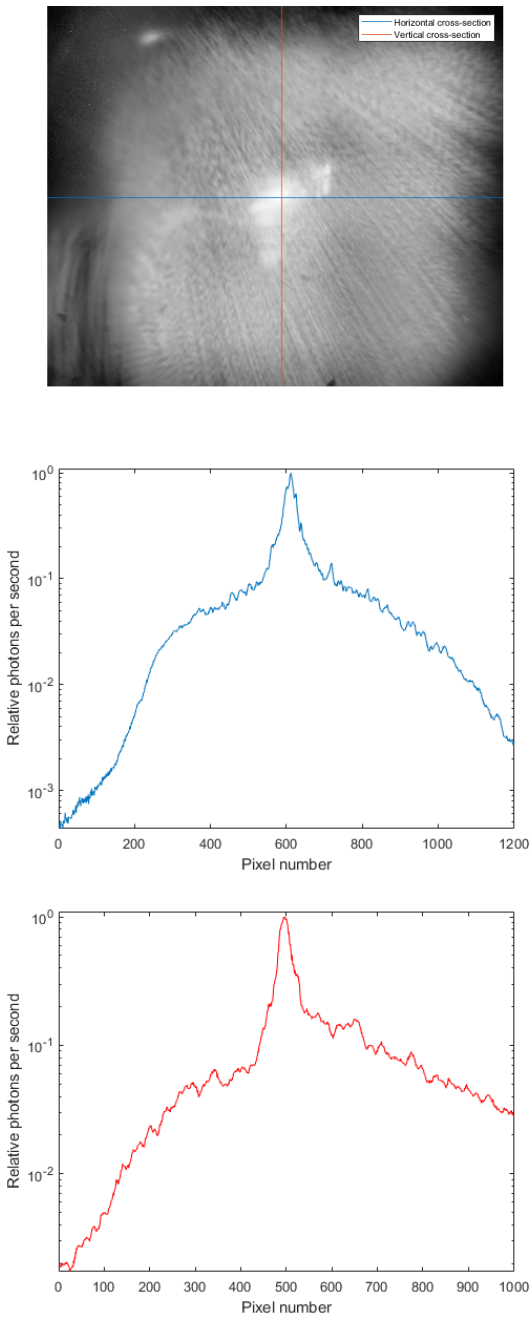

Figure 7: High dynamic range image (top), horizontal (centre) and vertical (bottom) cross-sections of the source point taken with stage 2 of the beam halo monitor using a 5 mm diameter Lyot stop.

losses will be higher than at present. First measurements have shown that the in-vacuum mirror causes a significant diffraction pattern to the bema halo images. An upgraded system featuring a Lyot stop demonstrated the diffraction contribution from the IVM can be significantly reduced, but not completely eliminated. Therefore further development is needed to confidently identify the degree of beam halo. For an improved beam halo monitor for Diamond-II, this work highlights that the IVM should be designed with minimal diffraction. Further improvements also include the use of post-processing to remove the remaining diffraction contribution from acquired images or the incorporation a micro mirror array to further suppress the point spread function. Further analysis could be done by comparing cross sections from the BHM with scraper measurements and simulations.

ACKNOWLEDGEMENTS

The authors would like to thank the Year in Industry programme at Diamond Light Source which funded this studentship.

REFERENCES

[1] R. Yang *et al.*, "Evaluation of beam halo from beam-gas scattering at the KEK Accelerator Test Facility", *Phys. Rev. Accel. Beams*, vol. 21, p. 051001, 2018. doi:10.1103/PhysRevAccelBeams.21.051001

[2] C. Thomas *et al.*, "X-ray pinhole camera resolution and emittance measurement", *Phys. Rev. ST Accel. Beams*, vol. 13, p. 022805, 2010. doi:10.1103/PhysRevSTAB.13.022805

[3] T. Mitsuhashi, "Beam Halo Observation by Coronagraph", in *Proc. DIPAC'05*, Lyon, France, Jun. 2005, paper ITMM03, pp. 7–11. https://jacow.org/d05/papers/ITMM03.pdf

[4] L.C. Chapon *et al.*, "Diamond-II Conceptual Design Report", May 2019. https://www.diamond.ac.uk/Home/About/Vision/Diamond-II.html

[5] A. Piwinski, "The Touschek Effect in Strong Focusing Storage Rings", DESY, pp. 98-179, 1999. arXiv:physics/9903034v1

[6] A. Goldblatt *et al.*, "Design and Performance of Coronagraph for for Beam Halo Measurments in the LHC", in *Proc. IBIC'16*, Barcelona, Spain, Sep. 2016, pp. 253–256. doi:10.18429/JACoW-IBIC2016-MOPG74

[7] J. Egberts and P. Welsch, "Flexible core masking technique for beam halo measurement swith high dynamic range", *J. Instrum.*, vol. 5, p. P04010, 2010. doi:10.1088/1748-0221/5/04/p04010

[8] H. D. Zhang *et al.*, "Beam halo imaging with a digital optical mask", *Phys. Rev. ST Accel. Beams*, vol. 15, p. 072803, 2012. doi:10.1103/PhysRevSTAB.15.072803

[9] J. Chouinard, "CCD vs CMOS industrial cameras", 2018. https://www.1stvision.com/machine-vision-solutions/2018/06/ccd-vs-cmos-industrial-cameras-excel-in-allied

[10] Black BORG Series, 2014. https://sciencecenter.net/hutech/catalog/bborg.pdf (accessed 3 September 2021)

[11] Edmund Optics Inc, "Allied Vision Mako G-319 1/1.8" Monochrome CMOS Camera", https://www.edmundoptics.com/p/allied-vision-mako-g-319-1-18-inch-monochrome-cmos-camera/33093/.

[12] QuickMTF, "Quick MTF, an image quality testing application", http://www.quickmtf.com/.

[13] MathWorks MATLAB, https://www.mathworks.com/products/matlab.html